Sequential integration of multi-omics data from serum improves the predictive performance of hepatic lipid accumulation in mice.

Martin David [1,2,*], Monbet Valérie [2], Leroyer Patricia [1,4], Oliviero Nolwenn [1], Turlin Bruno [1], Salim Zerrouki [3], Fautrel Alain [1], Ropert Martine [1,3,4], Sire Olivier [5], Loréal Olivier [1,4,*].

[1] UMR NuMeCan, INSERM U1317, INRAE U1341, University of Rennes, CHU of Rennes, Rennes, France
[2] University of Rennes, IRMAR UMR-CNRS 6625, Rennes, France
[3] Department of Biochemistry, University Hospital, Rennes, France
[4] AEM2 platform, University of Rennes and University Hospital of Rennes, France
[5] Bretagne Sud University, IRDL, CNRS 3744, Vannes, France
[*] Co-corresponding authors.

Co-corresponding authors:
David Martin, PhD, University of Rennes,
David.martin.2@univ.rennes.fr.

Olivier Loreal, MD, DR NuMeCan, INSERM,
Olivier.loreal@inserm.fr.

Keywords: Steatosis, Medical Prediction, Integration Strategy, Benchmark, Datasets.

THE BIGGER PICTURE.
The integration of multi-omics datasets for biomedical prediction remains a key challenge in precision medicine. While combining heterogeneous data types holds the promise of improving diagnostic accuracy, naïve fusion strategies often fail to capture the complementarity and complexity of biological systems fully. In this study, we introduce a new integration strategy that significantly enhances the prediction of hepatic lipid accumulation using minimally invasive serum data in a murine model. This work provides both a methodological advance and a reusable dataset, contributing a valuable resource for the development and validation of new machine learning pipelines in biomedicine.

SUMMARY.
Hepatic steatosis is a common feature of metabolic liver diseases and an early marker of disease progression. Non-invasive, accurate, and cost-effective tools are urgently needed for its detection and monitoring. In this study, we evaluated the predictive value of integrating three minimally invasive and complementary serum-derived datasets (routine biochemical markers, mid-infrared spectroscopy, and serum metallomic profiles) in a mouse model subjected to complex dietary and metabolic stressors. To address the challenges of multi-omics integration, we benchmarked several data fusion strategies and introduced a novel sequential integration method based on residual modelling. This approach incrementally captures complementary information from each dataset by focusing on the residual variability unexplained by previous models. Sequential integration consistently outperformed classical strategies and unimodal models, demonstrating improved predictive performance for hepatic lipid accumulation. The study offers both a generalizable integration strategy and a publicly available benchmark dataset, thereby paving the way for enhanced multi-omics prediction tools in biomedical research.

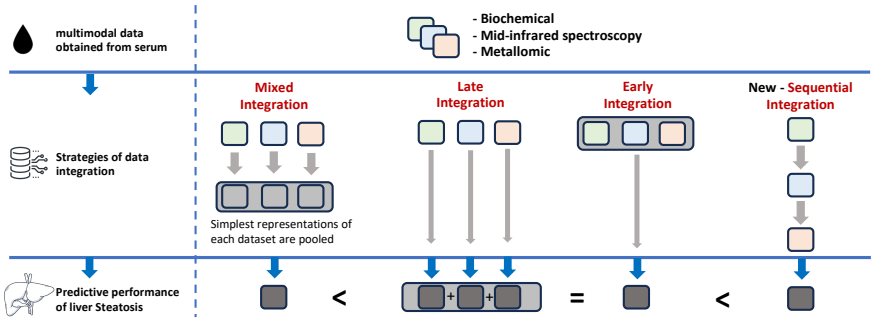

Graphical Abstract. Overview of multimodal data integration strategies for steatosis prediction.

INTRODUCTION

Metabolic Associated Fatty Liver Diseases (MAFLD) are one of the most common chronic liver diseases worldwide, affecting at least 10% of Europeans and 20% of the US population.[1] MAFLD mainly occurs in a context of obesity and/or metabolic syndrome, which associates, according to the International Diabetes Federation,[2] an abdominal obesity and at least two of the following factors: high triglyceride levels, low HDL cholesterol, hypertension treated or not, and high glycemia.[3] Such clinical features are facilitated by excessive food uptake, especially a Western diet, and a sedentary lifestyle. Hepatic steatosis, the first step of MAFLD, is characterized by an abnormal lipid accumulation within hepatocytes and may evolve with the appearance of hepatic lesions, such as hepatocyte ballooning and inflammation, that characterize the development of Metabolic Associated Steato-Hepatitis (MASH),[4] exposing to severe hepatic complications. Therefore, performing a diagnosis of hepatic steatosis stage is a major challenge for diagnosis and follow-up during therapeutic intervention.

To date, the histopathologic examination of liver biopsies remains the gold standard for staging and grading steatosis and evaluating complications. However, performing hepatic biopsy is an invasive and costly procedure, requiring short hospitalization for patients. It may induce abdominal pain and, in rarer cases, severe complications.[4–6] In this context, a minimally invasive, easy-to-perform, and inexpensive method for diagnosing steatosis and assessing its severity, as well as for monitoring in a large number of patients the effectiveness of therapeutic management, including nutritional recommendations, remains necessary.

Alternative tests have been proposed, including the evaluation of biological parameters determined *a priori* and imaging,[7,8] or the use of omics approaches, combined with machine learning algorithms.[9] Notably, recent studies proposed that a multimodal data approach (i.e., biochemistry, MRI, ultrasound, and elastometry) could improve the predictive performance.[10–12] We hypothesized that, by using deep learning, the use of a combination of three types of data easily acquired in patients through serum analysis could be effective in predicting hepatic steatosis. These parameters include: i)biochemical variables routinely determined in the serum during metabolic diseases staging, ii) mid-infrared (MIR) vibrational spectroscopy performed serum,[13] which give a metabolic profiling and has already been reported to be useful in evaluating the presence of hepatic steatosis,[14–16] iii) essential metals parameters in serum, including those that have been previously associated with MAFLD and/or the occurrence of steatotic liver, such as copper and iron.[17]

Therefore, our objective was to evaluate whether combining the three types of data, using tailored machine learning approaches, could improve the prediction efficacy of hepatic lipid accumulation. To this end, we employed a mouse model exposed to obesogenic diets, with or without iron supplementation, alongside their respective controls. This design introduced variability, reflecting a complex and realistic biological context, as observed in humans. We provide a rigorously curated benchmark of multimodal datasets characterized by this noisy clinical picture, which can serve as a resource for testing new machine learning models and bioinformatic pipelines. Within this framework, we evaluated various multimodal data integration strategies[18,19] and proposed a novel approach specifically designed to enhance the prediction of hepatic lipid accumulation in mice. Our results demonstrate that this sequential integration strategy significantly improves the predictive performance of the tested algorithms.

MATERIALS AND METHODS

Animals

Ninety-seven 8-week-old C57BL/6J male mice, obtained from Janvier Labs (Le Genet St Isle, France), were included. The protocol has been accepted by the Rennes Ethical Committee for animal experimentation studies (numéro). All mice were maintained in compliance with French law and regulations. Animals were randomly distributed into four groups. Two experimental variables were introduced: mice were subjected either to a control diet (D12328, 10 kcal% fat) or to a high-fat, high-carbohydrate (HFHC) diet (D12331; 58 kcal% fat diet and drinking water enriched with a mix of carbohydrates: 55% fructose and 45% sucrose, at a concentration of 42 g L^{-1}),[13,20] and, independently, received injections of iron-dextran (1 mg of Fe *per* g of body weight, two weeks after the beginning of the HFHC diet), or dextran alone.[21] The mice were fed *ad libitum* for 22 weeks and maintained in a temperature and light-controlled environment. After weighing, mice were anesthetized and sacrificed. Serum and the livers were then obtained and weighed. Parts of liver samples were quickly frozen in liquid nitrogen. Liver samples and serum were stored at -80°C until use. Part of the liver was also fixed in 4% buffered-formaldehyde for further histological studies.

Commenté [MOU1]: Il faut demander le numéro de saisine à Patricia.

Commenté [OL2]: Parle t'on d'autres organes dans le papier ?

Commenté [MOU3R2]: Non, j'ai modifié en ce sens.

Hepatic Histology

Formaldehyde-fixed biopsies were paraffin-embedded. Hemalun-eosin-safron (HES) and Sirius red staining were performed on 4 µm organ slices (UMS Biosit, Rennes, France). Histological assessments were performed by a liver pathologist (B.T.) in Rennes University Hospital and included quantification of hepatic steatosis, assessment of hepatic inflammation, and evaluation of hepatic fibrosis. Fibrosis was scored from 0 to 4. Inflammatory foci were quantified and normalized to the liver surface of the tissue section. Steatosis was investigated on HES-stained slices by quantifying the percentage of hepatocytes containing steatotic vesicles.

Commenté [OL4]: Peut être plus d'éléments sur le staging. Voir si Bruno est OK

Commenté [MOU5R4]: On peut, peut-être citer une publication de Bruno sur la manière de faire.

Hepatic triglyceride quantification

Hepatic triglyceride concentrations (HTG) were quantified using the DiaSys kit (Diagnostic System, Grabels, France) previously described.[22] Briefly, 30-50 mg of liver homogenate was extracted with a methanol-chloroform-H_2O (2/1/2) mixture. The organic layers were collected after centrifugation and dried under nitrogen. Dry samples were reconstituted in isopropanol/acetonitrile/water (1/1/2) mixture and then analyzed according to the manufacturer's recommendations.

Hepatic gene expression measurement

hepatic total RNAs were extracted following the procedure of the Nucleospin RNA Plus (Macherey Nagel) extraction kit and then measured with the Spectrometer ND-1000 (Nanodrop). Then, quantitative PCRs were performed using 384-well plates, with 2 µl of sample, 1 µl of forward primer, then 1 µl of reverse primer, 5 µl of Sybr Green 1 (Eurogentec, Liège, Belgium), and 1µl of water RNAase-free *per* well (7900 HT Fast Real-Time PCR System). The housekeeping gene used was Hypoxanthine Phosphoribosyl Transferase 1 (*Hprt1*). The mRNA levels of genes involved in the inflammatory process – C-reactive protein (*Crp*) and α2-macroglobulin (*A2m*) were evaluated. Oxidative stress was investigated by quantifying the mRNA levels of nuclear factor erythroid 2-related factor 2 (*Nrf2*), a master gene in the defense against oxidative stress. *Fsp27* mRNA level was also evaluated. It is reported as a direct marker of steatosis.[23] Primers used for quantitative PCR are indicated in Table S2.

Mulli-omics datasets

1) *Serum biochemical markers [dataset n°1].* The following biochemical markers were measured in serum using the methods routinely used in the Biochemistry Department at the Rennes University

Hospital: glucose, aspartate aminotransferase (ASAT), alanine aminotransferase (ALAT), serum triglycerides, total cholesterol, serum iron, and UIBC as previously described.[24,25]

2) *Mid-infrared spectra acquisition and preprocessing [dataset n°2].* 94 serums were available for MIR analyses. MIR spectra were recorded using a Mid-infrared Lumos microspectrophotometer (Bruker) equipped with a MCT detector following the previously described procedure.[26] Then, MIR spectra were pre-processed in the 3500-800 cm^{-1} frequency domain. Second derivatives were calculated, smoothed using a 13–point Savitzky-Golay algorithm and vector normalized. Then, they were subjected to a multi-resolution β −spline data compression.[26]
3) *Serum Metallome [dataset n°3]* The elements studied were either essential - manganese (Mn), iron (Fe), copper (Cu), cobalt (Co), zinc (Zn), selenium (Se), rubidium (^{85}Rb), molybdenum (Mo), or toxic -arsenic (As), cadmium (Cd), tin (^{119}Sn), lead (^{207}Pb). All these were measured, as previously reported **REF**, by Inductively Coupled Plasma Mass Spectrometry (ICP-MS) in a X-Series II from Thermo Scientific equipped with collision cell technology (Platform AEM2, Biochemical Laboratory, Rennes University – Rennes hospital). The source of plasma was argon (purity degree > 99.99%). The collision/reaction cell used was pressurized with a mixture of helium (93%) and hydrogen (7%); Messer provided argon and hydrogen. Ultra-pure water was provided from the Millipore Direct-Q 3 water station. Nitric acid solution utilized at 69% (Fisher Chemical – Optima Grade). Rhodium was used as an internal standard (Fisher Scientific). Calibration ranges were realized using a multi-element solution (SCP Science Plasma Cal). The performance was calibrated using multi-element solutions, tune F and tune A (Thermo). Certified reference material bovine liver ZC71001 was obtained from NCS Testing Technology (Beijing, China). When a metal concentration was below the limit of quantification of the method, the value was arbitrarily indicated as 0.

Commenté [OL6]: Voir ce qui a été dosé ou utilisé pour la formulation du texte. On en parle à ton retour et avec Martine. Je ne sais plus si c'était avant ou après le changement de machine.

Commenté [MOU7R6]: Tous ceux qui sont sur la figure S4.

Statistical analysis

All statistical analyses and the entire code are available in a corresponding repository: https://github.com/DJrMartin/Multimodale_data_for_prediction.git.

1) *Descriptive analyses.* The results of histological and biochemical measurements are presented as mean ± standard deviation. Non-parametric tests (Kruskal–Wallis and Dunn's multiple comparison tests with Bonferroni correction) were used to estimate significance as appropriate. *p*-values < 0.05 were considered significant without Bonferroni correction.
2) *Mantel test.* To assess the correlation between distance matrices derived from different datasets, Mantel tests were performed. This non-parametric test evaluates the statistical significance of the association between two distance matrices, based on Pearson's correlation coefficient and 999 permutations. Mantel tests were applied to explore the shared information between omics-based distances and steatosis.
3) *Overview of the integration strategies.* Several integration strategies are available to integrate the previously presented multi-omics datasets.[18,19] (i) Early Integration means the sample concatenation of datasets. (ii) Mixed Integration aims to reduce data complexity through independent (robust or kernel PCA) transformations. (iii) Intermediate integration also aims to reduce data complexity through joint transformations (Canonical Correlations Analysis). (iv) Late Integration processes each dataset separately, combining predictions post hoc using a linear model. Hierarchical Integration (v) exploits known regulatory relationships between omics layers.
4) *New strategy: Sequential Integration (vi).* We develop a new approach based on a series of random forests, which is based on the Ensemble Learning approach.[27,28] First, a random forest is fitted on a unique dataset. Then the next random forest is optimized to reduce the residual error of the first model, and et cetera (Graphical Abstract). The description of the algorithm is available in Algorithm

Commenté [OL8]: Dire ici quelles données ont été intégrées pour modéliser

Commenté [MOU9R8]: J'ai harmonisé le paragraphe précédent pour comprendre les 3 jeux de données que l'on utilise et modifié la phrase en ce sens.

Commenté [OL10]: Homogeneiser par rapport au graphical abstracr

Commenté [MOU11R10]: Non car le graphical abstract classe les methodes par performance. Ici on les classe comme la littérature.

1. Hyperparameters, such as maximum tree depth and the maximum number of nodes, were tuned for each type of dataset using cross-validation. Feature importance scores were extracted from each model to identify key predictors contributing to the regression task for each dataset. Model performance was evaluated using repeated cross-validation (30-fold) to ensure robust estimation of predictive performance. Each predictive model was constructed using a random selection of 70% of the total population and validated with the remaining 30% of the total population. The distribution of the performance metric (Root Mean Square Error) is presented in the form of a boxplot.

Commenté [OL12]: ?

Commenté [MOU13R12]: Il était à la fin du papier, mais je l'ai ajouté ici à la suite pour la fluidité.

Algorithm 1: Sequential Integration.

Let:

- $\boldsymbol{y} \in \mathbb{R}^n$, the target variable (i.e., steatosis).
- $\{X^{(1)}, X^{(2)}, \ldots, X^{(M)}\}$, a list of datasets with the same number of rows n.
- K, the number of cross-validation folds.

For each fold, $k = 1, \ldots, K$:

1. Randomly split data into training and test sets.
2. Initialize residuals:

$$r^{(1)} = y_{train}.$$

3. For each dataset, $m = 1, \ldots, M$:
   - Train a random forest model $\mathrm{f}^{(\mathrm{m})}$ to predict $r^{(m)}$.
   - Update residuals:

$$r^{(m+1)} = r^{(m)} - f^{(m)}\left(X_{train}^{(m)}\right).$$

4. Compute test prediction as:

$$y_{test} = \sum_{m=1}^{M} f^{(m)}\left(X_{test}^{(m)}\right).$$

5. Compute RMSE:

$$RMSE^{(k)} = \sqrt{\frac{1}{n_{test}^{(k)}} \sum_{i \in X_{test}^{(k)}} (y_i - y_i)^2}.$$

RESULTS

Both the HFHC diet and iron supplementation induce intra- and intergroup heterogeneity in the development of hepatic steatosis.

The experimental design permits to induce of heterogeneity in the spectrum of liver steatosis and iron excess (Figure S1), with corresponding representative histological slides in Figure S2. In this study, the steatosis (i.e., hepatic lipid accumulation) has been evaluated through 3 biological approaches: (i) the histological score, which is the gold standard, informs about the steatosis (Figure 1A), (ii) the quantitative hepatic triglyceride (TG) content (Figure 1B), and (iii) the mRNA level of *Fsp27* (Figure 1C) recognized as a direct marker of steatosis).[23]

The HFHC diet induced an increase in: (i) histological hepatic steatosis, compared with the CTL and IRON groups (+40% cells and +36% cells, respectively, Figure 1A); (ii) the hepatic TG concentration compared with CTL and IRON groups (+204% for both groups, Figure 1B); (iii) the *Fps27* mRNA level compared with CTL and IRON groups (+90% and +105%, respectively, Figure 1C).

Combined HFHC diet and iron supplementation also led to (i) an increase in hepatic steatosis compared with CTL and IRON alone groups (+14% of cells and +9% of cells, respectively, Figure 1A), but a decrease compared to HFHC diet alone (-27% of cells, $p<0.05$, Figure 1A), (ii) an increase in hepatic TG concentration compared with CTL and IRON alone groups (+153% for both groups, Figure 1B), but a decrease compared to HFHC diet alone (-17%, Figure 1B), (iii) an increase in mRNA level of Fsp27 compared with CTL and IRON alone groups (+11% and +20%, respectively, Figure 1C), but a decrease compared to HFHC diet alone (-42%, Figure 1C). Noteworthy, in each of the HFHC groups, there was also a strong heterogeneity, which adds to the intergroup variability, despite the similar regimen from one animal to another within the group.

The intergroup variability is also found regarding animal weight. Whereas the HFHC diet shows a strong weight gain, the supplementation by iron (IRON + HFHC group) partially blunts this effect, suggesting a non-linear interaction between dietary fat and parenteral iron overload (Table 1). Similarly, the effects of iron alone (IRON group) on liver mass -an increase- or adipose tissue – a decrease- differ from those observed under the HFHC diet, and in some cases show opposing trends (i.e., peri-epididymal fat was reduced with iron alone but increased under HFHC). This divergence extends also to biochemical markers such as transferrin saturation, serum iron, and triglycerides, which are differentially modulated by diet and iron, with effects that are synergistic or antagonistic regarding the parameter (Table 1). Liver ASAT level is also elevated in the presence of iron, highlighting the complexity and potential hepatotoxic effects of iron supplementation (Table 1). Altogether, iron excess acts as a source of experimental noise, altering the expected effects of the obesogenic diet and increasing heterogeneity in the dataset.

Definition of an integrated parameter representative of hepatic steatosis level

While histological quantification remains the gold standard, a notable discrepancy was observed between the three biological scale assessments of hepatic lipid accumulation. As shown in Figure 1D, within the range of 20 to 40 mg of triglycerides per gram of liver, which can be considered as an early stage of lipid accumulation, histological scoring fails to detect a clear increase in hepatic lipid accumulation (between dashed lines in Figure 1D).

In the context of machine learning prediction, the question remains about the choice of the *right* target variable that we need to predict. Therefore, to take into account the hepatic lipid accumulation

Commenté [OL14]: Peut-être le Perls ? surement

Commenté [MOU15R14]: On n'en parle pas en discussion.

Commenté [OL16]: Discutons-nous bien de l'intérêt de cela dans la discussion

Commenté [MOU17R16]: Tu parles du bruit expérimental ?? si c'est le cas, oui nous en discutons.

Commenté [OL18]: Que sont les 2 points flottants sous 20 mg du groupe iron ?

Commenté [MOU19R18]: Des souris avec un stéatose micro-vésiculaire donc plutôt stress intracellulaire et non accumulation de graisses. .

evaluated by the three biological scales, a synthetic variable that sums up hepatic lipid accumulation was defined. A principal component analysis (PCA) has been performed integrating the three indicators of lipid accumulation in the liver: (i) histological steatosis, (ii) Hepatic triglyceride content, and the mRNA level of hepatic *Fsp27 mRNA*.

We first validate the interpretation of the Principal Components (PC) of the PCA by calculating confidence intervals for Pearson's correlation coefficients between the coordinates and the variables measured in each mouse (Figure 1E). The first principal component (PC1) is consistently associated with all markers of liver lipid accumulation, indicating that higher PC1 scores correspond to more severe hepatic steatosis (Figure 1E, Panel 2). This interpretation is supported by a positive association with an increase in alanine aminotransferase (ALAT) levels and the inverse relationship with the ASAT/ALAT ratio (p<0.05, Figure 1E, Panel 1), consistent with a potential diet-induced liver damage.[29] On this basis, we select the coordinates in PC1 as the main outcome variable that we have to predict.

A multi-modal approach appears essential to encompass all the information in the dataset.
In this study, we constructed several datasets. The first dataset consists of biochemical measurements from serum. All biochemical data, stratified by experimental condition, are presented in Table 1. The second dataset is derived from MIR spectroscopy performed on serum, providing molecular fingerprints specific to each mouse. Representative pre-processed spectra, depending on experimental groups, are represented in Figure S3. The third dataset comprises quantitative measurements of metals and trace elements in the blood, presented in Figure S4.

The goal here is to assess the redundancy or non-redundancy of information between types of data and the predictive potential of each type of data for steatosis. We compute (i) the pairwise sample distance matrix from the three variables summarizing hepatic lipid accumulation, (ii) the pairwise sample distance matrix from one type of data, and finally, we perform (iii) a Mantel test comparing both pairwise sample distance matrices. The Mantel test evaluates the correlation between two distance matrices. The test produces a distribution of Pearson's correlation coefficient (r), which quantifies the strength and direction of the linear relationship between corresponding distances in the two matrices. A high positive Pearson's r indicates that the two datasets capture similar patterns of variation among the samples (i.e., samples that are similar in one dataset tend to be similar in the other as well).

Here, we show that the serum biochemical markers exhibit the highest similarity in sample structure to the variables describing liver steatosis. Both the MIR and metallomic datasets also demonstrate significant associations with lipid accumulation-related variables (Figure 2A). We also perform the Mantel test to compare the degree of sharing information between types of data. Figure 2B reveals that the MIR dataset shares limited information with the serum biochemistry data. However, the metallomic dataset appears to share more information with serum markers, suggesting potential redundancy. These observations suggest that (i) each dataset contains predictive information relevant to steatosis (Figure 2A), and (ii) each dataset provides distinct and potentially complementary insights (Figure 2B). In this context, we propose to apply different integration strategies to the three types of data to effectively leverage complementary, non-redundant information distributed across datasets.

A novel integration strategy, named Sequential Integration, improves the predictive performance of steatohepatitis in the mouse model.

Commenté [OL20]: Lesquels ?

Commenté [MOU21R20]: L'ensemble des variables, c'est un test multivarié.

Commenté [OL22]: Lesquelles ?

Commenté [MOU23R22]: Pareil l'ensemble des variables décrivant la steatose.

Commenté [OL24]: Il faut être sur que ce n'est pas proposé dans d'autres domaines ?

Commenté [MOU25R24]: Vérifié.

We develop predictive models for the synthetic variable representing hepatic steatosis in mice, aiming to identify the best multi-omics data integration strategy to improve prediction. The predictive performance is evaluated by computing the Root Mean Squared Error (RMSE). A lower RMSE indicates better predictive performance. Moreover, to benchmark the performance of each strategy, we estimate a random prediction baseline (grey box, Figure 3A); models with a lower RMSE possess the highest predictive performance. Detailed methods are in the Materials and Methods section.

Commenté [MOU26]: Je n'arrive pas à retrouver ce qui est écrit dans la figure. Il faut que l'on voit cela.

Commenté [MOU27R26]: Je. Ne vois pas comment faire mieux.

First of all, we assess predictive values independently for each data type (Figure 3A). Among the unimodal models, this based on serum biomarker profiles, demonstrates the highest predictive performance ($RMSE_{unimodal}$ = 0.98 $^{(\pm 0.18)}$, Figure 3A). From now on, this unimodal approach (coloured in light green in Figure 3A) serves as a reference to evaluate the benefits of multi-omics integration. In this context, boxplots in red in Figure 3 mean that the RMSE is higher than the RMSE based on serum biomarker profiles, while boxplots in blue mean that the predictive performance of the model outperforms this based on serum biomarkers.

The predictive performances of the Early, Late, and Mixed integrations are presented respectively in Figures 3B ($RMSE_{early}$ = 0.94 $^{(\pm 0.18)}$ for XtremGB and 0.97 $^{(\pm 0.18)}$ for RF), 3C ($RMSE_{late}$ = 0.99 $^{(\pm 0.16)}$), and 3D ($RMSE_{mixed}$ = 1.19 $^{(\pm 0.18)}$ for K.PCA and 1.19 $^{(\pm 0.21)}$ for R.PCA). These strategies do not enhance predictive performance compared to the reference model (in light green, Figure 3A); even the Mixed integration approaches perform worse than the reference model ($p < 0.05$).

To overcome the limitations of naive integration, we propose a sequential integration strategy based on a residual learning framework.[30] In this approach, models are trained in sequence, with each model learning to predict the residuals (i.e., the unexplained variability) of the previous one (as it is presented in Algorithm 1). Predictive performance of sequential data integration, presenting the lowest RMSE, is the one that integrates the data in that order: Biomarkers/Metallome/MIR (i.e., $RMSE_{seq}$ = 0.84 $^{(\pm 0.17)}$, Figure 3E). It presents higher performances compared to other integration strategies ($p < 0.05$). It also appears that the integration of 2 datasets seems sufficient to improve the predictive performance. Overall, our results demonstrate that this residual-based modelling approach outperforms all unimodal models, including those relying solely on serum markers (Figure 3A and 3E). By changing the order of the multi-omics data integration at each step, we show that the order in which data types are integrated does not appear to significantly affect predictive performance (Figure 3E).

The model based on the sequential integration is interpretable.

Analysis of the most influential variables from the sequential multi-omics integration reveals that each data modality contributes distinct and biologically meaningful information. These results are summarized in Table 2. Notice that the important variables reported here are provided by the greatest model of the sequential integration (Biomarkers/Metallome/MIR). The statistical construction of the model means that, for instance, wavenumbers highlighted by the model bring non-redundant and complementary information to previously highlighted variables (biomarkers and metallome) in the previous model.

Interestingly, among classical serum markers, our model highlights that cholesterol seems positively associated with hepatic lipid accumulation. It is in line with established clinical indicators.[31,32] Regarding metallomic data, increased variations in zinc and copper levels were among the most

predictive features, highlighting the role of trace metal homeostasis in liver pathology (Table 2). Those element traces have already been associated with hepatic lipid accumulation.[17]

Finally, in the MIR spectral data, specific wavenumber regions related to glucose absorption emerged as key predictors (i.e., wavenumbers between 1300 and 900 cm^{-1}, Table 2).[33] The importance of each MIR wavenumber from the sequential model (Biomarkers/Metallome/MIR) is also illustrated in Figure S3. Among the wavenumbers highlighted, four regions were particularly informative. The 1230 cm^{-1} band, attributed to P=O and C–O vibrations, reflected contributions from nucleotides, phospholipids, and organic phosphates.[33] The combined signals at 1180 and 950 cm^{-1}, corresponding to C–O/C–C stretching and sugar ring vibrations, were linked to simple sugars (glucose, lactate, pyruvate), cyclic carbohydrates, ribose, and phosphorylation-related structures, pointing to changes in carbohydrate metabolism.[34,35] Finally, the 840 cm^{-1} band, assigned to C–H out-of-plane bending in ring structures, indicated contributions from nucleic acids, polysaccharides, and cyclic proteins.[36]

Therefore, the model constructed through sequential integration aligns with established literature, confirming both the potential and the promising applicability of this approach.

DISCUSSION

The objective of this study was to set up a novel method allowing to predict the lipid accumulation in the liver using minimally invasive, by integrating routinely accessible data, aiming to reduce the reliance on hepatic biopsy.

To achieve this, we designed a study in mice in which two qualitative variables were manipulated to generate a highly heterogeneous clinical landscape, resulting in varying degrees of hepatic lipid accumulation. Indeed, our data shows that in addition to heterogeneity within groups submitted to the HFHC diet, the addition of iron increased phenotypic variability, which introduces noise into the biological signatures, thus making prediction more challenging. In this respect, our experimental design is innovative in order to improve the robustness of the prediction.

A second key innovation lies in the multimodal biomarker profiling. We quantified three distinct types of information: classical serum markers, mid-infrared spectral metabolic signatures of serum, and metal concentrations in serum. Despite being derived from the same biological fluid, these datasets were shown to carry complementary and non-redundant information. As the datasets have been made publicly available, they can be used to test new machine learning pipelines or bioinformatic approaches.

In this context, we test different integration strategies to predict the liver status of mice. We first demonstrate that current multimodal data integration does not outperform predictive performance and that the choice of integration strategy significantly impacts model outcomes, depending on the nature of the data. For example, mixed integration strategies, which aim to project all datasets into a latent space, may discard information that is specific to predict hepatic lipid accumulation.

A seemingly straightforward alternative is early integration, which concatenates all features into a single large dataset. While gradient boosting algorithms can, in theory, exploit such combined information by fitting successive models to refine predictions,[30] we found this strategy suboptimal. This is likely due to the heterogeneous nature of the datasets: for instance, mid-infrared spectral data

contain over 1,500 highly correlated variables (wavenumbers), unlike the metallomic data, which are sparser and less redundant. Gradient boosting methods are sensitive to the initial data structure and hyperparameters (e.g., number of trees), and this heterogeneity poses challenges.

To address these limitations, we developed a novel integration approach based on residual modelling. In this sequential strategy, a predictive model (e.g., random forest or gradient boosting) is trained on one data modality, and the subsequent model is trained to predict the residuals (unexplained variance) of the previous model using a different data modality. Each step thus focuses on the information not captured by earlier models, allowing each data type to contribute complementary insights. Crucially, this strategy allows model parameters to be tailored to the characteristics of each dataset, leading to improved overall predictive performance.

Here, we show that the sequential strategy outperforms all the other integration strategies (Figure 3). It does not mean that this approach is relevant for all biological problems, but it seems that it is for multimodal datasets showing a very different kind of nature.[37] For instance, diagnosis involves compositional data derived from gut microbiota composition, and serum biomarkers should use this approach.[38]

CONCLUSIONS

Our findings underscore the critical role of integration strategies in enhancing the predictive performance of multimodal omics data for assessing clinical conditions such as steatosis. The use of serum-based biochemical, MIR, and metallomic data, combined through appropriate integration methods, offers a non-invasive, cost-effective alternative to current diagnostic tools, such as liver biopsy or imaging. This approach holds promise for clinical translation, particularly for early detection, stratification, and longitudinal monitoring of steatosis in humans. Furthermore, beyond prediction, we propose a benchmark of multimodal datasets that can be reused to test innovative predictive methodologies.

RESSOURCE AVAILABILITY

Led contact

Requests for further information and resources should be directed to and will be fulfilled by the lead contact, Martin David (David.martin.2@univ-rennes.fr).

Materials availability

This study did not generate new unique reagents.

Data and code availability

All datasets and the source code used in this study are publicly available on GitHub: https://github.com/DJrMartin/Multimodale_data_for_prediction.git.

Acknowledgments

This work was supported by the Agri-Food Carnot Institute.

Author's contributions

David Martin, Conceptualization, Statistical analysis, Investigation, Methodology, Writing. **Valérie Monbet,** Conceptualization, Statistical analysis, Investigation, Methodology, Writing, **Patricia Leroyer**, Animal experiment, biological assays, Technical support, **Nolwenn Oliviero**, Animal experiments,

biological assays, technical support, **Bruno Turlin**, Pathologist, Hepatic histological quantification, **Alain Fautrel**, Methodology, **Martine Ropert**, Biochemical analysis, **Salim Zerrouki,** Biochemical analysis. **Olivier Sire**, Spectral acquisition, Investigation, Methodology, Writing, **Olivier Loréal**, Conceptualization, Obtention of financial support, Investigation, Animal experimentation, Methodology, Writing.

Declaration of interests
The authors declare no competing interests.

Supplemental information
Supplemental information can be found online at [link].

REFERENCES

1. Estes, C., Razavi, H., Loomba, R., Younossi, Z., and Sanyal, A.J. (2018). Modeling the epidemic of nonalcoholic fatty liver disease demonstrates an exponential increase in burden of disease. Hepatology *67*, 123–133. https://doi.org/10.1002/hep.29466.

2. Bener, A., Zirie, M., Musallam, M., Khader, Y.S., and Al-Hamaq, A.O.A.A. (2009). Prevalence of Metabolic Syndrome According to Adult Treatment Panel III and International Diabetes Federation Criteria: A Population-Based Study. Metabolic Syndrome and Related Disorders *7*, 221–230. https://doi.org/10.1089/met.2008.0077.

3. Grundy, S.M., Cleeman, J.I., Daniels, S.R., Donato, K.A., Eckel, R.H., Franklin, B.A., Gordon, D.J., Krauss, R.M., Savage, P.J., Smith, S.C., et al. (2005). Diagnosis and Management of the Metabolic Syndrome. Circulation *112*, e285–e290. https://doi.org/10.1161/CIRCULATIONAHA.105.169405.

4. Matteoni, C.A., Younossi, Z.M., Gramlich, T., Boparai, N., Liu, Y.C., and McCullough, A.J. (1999). Nonalcoholic fatty liver disease: a spectrum of clinical and pathological severity. Gastroenterology *116*, 1413–1419. https://doi.org/10.1016/s0016-5085(99)70506-8.

5. Bedossa, P., Poitou, C., Veyrie, N., Bouillot, J.-L., Basdevant, A., Paradis, V., Tordjman, J., and Clement, K. (2012). Histopathological algorithm and scoring system for evaluation of liver lesions in morbidly obese patients. Hepatology *56*, 1751–1759. https://doi.org/10.1002/hep.25889.

6. Kleiner, D.E., Brunt, E.M., Van Natta, M., Behling, C., Contos, M.J., Cummings, O.W., Ferrell, L.D., Liu, Y.-C., Torbenson, M.S., Unalp-Arida, A., et al. (2005). Design and validation of a histological scoring system for nonalcoholic fatty liver disease. Hepatology *41*, 1313–1321. https://doi.org/10.1002/hep.20701.

7. Castera, L., Friedrich-Rust, M., and Loomba, R. (2019). Noninvasive Assessment of Liver Disease in Patients With Nonalcoholic Fatty Liver Disease. Gastroenterology *156*, 1264-1281.e4. https://doi.org/10.1053/j.gastro.2018.12.036.

8. Vilar-Gomez, E., and Chalasani, N. (2018). Non-invasive assessment of non-alcoholic fatty liver disease: Clinical prediction rules and blood-based biomarkers. J Hepatol *68*, 305–315. https://doi.org/10.1016/j.jhep.2017.11.013.

9. Wong, V.W.-S., Adams, L.A., de Lédinghen, V., Wong, G.L.-H., and Sookoian, S. (2018). Noninvasive biomarkers in NAFLD and NASH — current progress and future promise. Nat Rev Gastroenterol Hepatol *15*, 461–478. https://doi.org/10.1038/s41575-018-0014-9.

10. Keegan, A., Malamal, G., Lee, Y., Korolowicz, K., Shepard, B.D., Ecelbarger, C.M., Rubiano, M.M., Avantaggiati, M.L., Levi, M., Rich, L., et al. (2025). Multimodal Diagnostic Imaging of Metabolic Dysfunction–Associated Steatotic Liver Disease: Noninvasive Analyses by Photoacoustic Ultrasound and Magnetic Resonance Imaging. The American Journal of Pathology *195*, 875–890. https://doi.org/10.1016/j.ajpath.2025.01.012.

11. Ribeiro, R.T., Marinho, R.T., and Sanches, J.M. (2013). Classification and Staging of Chronic Liver Disease From Multimodal Data. IEEE Transactions on Biomedical Engineering *60*, 1336–1344. https://doi.org/10.1109/TBME.2012.2235438.

12. Wei, X., Wang, Y., Wang, L., Gao, M., He, Q., Zhang, Y., and Luo, J. (2024). Simultaneous grading diagnosis of liver fibrosis, inflammation, and steatosis using multimodal quantitative ultrasound and artificial intelligence framework. Med Biol Eng Comput. https://doi.org/10.1007/s11517-024-03159-z.

13. Le Corvec, M., Allain, C., Lardjane, S., Cavey, T., Turlin, B., Fautrel, A., Begriche, K., Monbet, V., Fromenty, B., Leroyer, P., et al. (2016). Mid-infrared fibre evanescent wave spectroscopy of serum allows fingerprinting of the hepatic metabolic status in mice. Analyst *141*, 6259–6269. https://doi.org/10.1039/c6an00136j.

14. Anne, M.-L., Le Lan, C., Monbet, V., Boussard-Plédel, C., Ropert, M., Sire, O., Pouchard, M., Jard, C., Lucas, J., Adam, J.L., et al. (2009). Fiber evanescent wave spectroscopy using the mid-infrared provides useful fingerprints for metabolic profiling in humans. J Biomed Opt *14*, 054033. https://doi.org/10.1117/1.3253319.

15. Le Corvec, M., Jezequel, C., Monbet, V., Fatih, N., Charpentier, F., Tariel, H., Boussard-Plédel, C., Bureau, B., Loréal, O., Sire, O., et al. (2017). Mid-infrared spectroscopy of serum, a promising non-invasive method to assess prognosis in patients with ascites and cirrhosis. PLoS One *12*, e0185997. https://doi.org/10.1371/journal.pone.0185997.

16. Anty, R., Morvan, M., Le Corvec, M., Canivet, C.M., Patouraux, S., Gugenheim, J., Bonnafous, S., Bailly-Maitre, B., Sire, O., Tariel, H., et al. (2019). The mid-infrared spectroscopy: A novel non-invasive diagnostic tool for NASH diagnosis in severe obesity. JHEP Rep *1*, 361–368. https://doi.org/10.1016/j.jhepr.2019.09.005.

17. Aigner, E., Weiss, G., and Datz, C. (2015). Dysregulation of iron and copper homeostasis in nonalcoholic fatty liver. World J Hepatol *7*, 177–188. https://doi.org/10.4254/wjh.v7.i2.177.

18. Picard, M., Scott-Boyer, M.-P., Bodein, A., Périn, O., and Droit, A. (2021). Integration strategies of multi-omics data for machine learning analysis. Computational and Structural Biotechnology Journal *19*, 3735–3746. https://doi.org/10.1016/j.csbj.2021.06.030.

19. Li, Y.C., Wang, L., Law, J.N., Murali, T.M., and Pandey, G. (2022). Integrating multimodal data through interpretable heterogeneous ensembles. Bioinformatics Advances *2*, vbac065. https://doi.org/10.1093/bioadv/vbac065.

20. Xin, X., Cai, B.-Y., Chen, C., Tian, H.-J., Wang, X., Hu, Y.-Y., and Feng, Q. (2020). High-trans fatty acid and high-sugar diets can cause mice with non-alcoholic steatohepatitis with liver fibrosis and potential pathogenesis. Nutr Metab (Lond) *17*, 40. https://doi.org/10.1186/s12986-020-00462-y.

21. Martin, D., Nay, K., Robin, F., Rebillard, A., Orfila, L., Martin, B., Leroyer, P., Guggenbuhl, P., Dufresne, S., Noirez, P., et al. (2022). Oxidative and glycolytic skeletal muscles deploy protective mechanisms to avoid atrophy under pathophysiological iron overload. J cachexia sarcopenia muscle *13*, 1250–1261. https://doi.org/10.1002/jcsm.12897.

22. Appriou, Z., Nay, K., Pierre, N., Saligaut, D., Lefeuvre-Orfila, L., Martin, B., Cavey, T., Ropert, M., Loréal, O., Rannou-Bekono, F., et al. (2019). Skeletal muscle ceramides do not contribute to physical inactivity-induced insulin resistance. Applied Physiology, Nutrition, and Metabolism *44*, 1180–1188. https://doi.org/10.1139/apnm-2018-0850.

23. Matsusue, K., Kusakabe, T., Noguchi, T., Takiguchi, S., Suzuki, T., Yamano, S., and Gonzalez, F.J. (2008). Hepatic Steatosis in Leptin-Deficient Mice Is Promoted by the PPARγ Target Gene Fsp27. Cell Metabolism *7*, 302–311. https://doi.org/10.1016/j.cmet.2008.03.003.

24. Horeau, M., Navasiolava, N., Van Ombergen, A., Custaud, M.-A., Robin, A., Ropert, M., Antunes, I., Bareille, M.-P., Billette De Villemeur, R., Gauquelin-Koch, G., et al. (2024). Dry immersion rapidly disturbs iron metabolism in men and women: results from the VIVALDI studies. npj Microgravity *10*, 68. https://doi.org/10.1038/s41526-024-00399-z.

25. Horeau, M., Ropert, M., Mulder, E., Tank, J., Frings-Meuthen, P., Armbrecht, G., Loréal, O., and Derbré, F. (2022). Iron metabolism regulation in females and males exposed to simulated microgravity: results from the randomized trial Artificial Gravity Bed Rest—European Space Agency (AGBRESA). The American Journal of Clinical Nutrition *116*, 1430–1440. https://doi.org/10.1093/ajcn/nqac205.

26. Martin, D., Monbet, V., Sire, O., Corvec, M.L., and Loréal, O. (2021). Multi-resolution B-splines data compression improves MIR spectroscopy-based Health diagnostic efficiency. Talanta Open *4*, 100063. https://doi.org/10.1016/j.talo.2021.100063.

27. Dietterich, T.G. (2000). Ensemble Methods in Machine Learning. In Multiple Classifier Systems (Springer), pp. 1–15. https://doi.org/10.1007/3-540-45014-9_1.

28. Opitz, D., and Maclin, R. (1999). Popular Ensemble Methods: An Empirical Study. Journal of Artificial Intelligence Research *11*, 169–198. https://doi.org/10.1613/jair.614.

29. Nyblom, H., Berggren, U., Balldin, J., and Olsson, R. (2004). High AST/ALT ratio may indicate advanced alcoholic liver disease rather than heavy drinking. Alcohol Alcohol *39*, 336–339. https://doi.org/10.1093/alcalc/agh074.

30. Friedman, J.H. (2001). Greedy function approximation: A gradient boosting machine. The Annals of Statistics *29*, 1189–1232. https://doi.org/10.1214/aos/1013203451.

31. Lonardo, A. (2024). Alanine aminotransferase predicts incident steatotic liver disease of metabolic etiology: Long life to the old biomarker! World J Gastroenterol *30*, 3016–3021. https://doi.org/10.3748/wjg.v30.i24.3016.

32. Elsawy, A.A., Hodeib, H., Selim, A.F., Sarhan, M.E., Elhadidy, A.A., Sameir, H.M., Selim, A., and Tawfik, M.A. (2023). The possible association between blood level of free cholesterol and the severity of steatosis in patients with nonalcoholic fatty liver disease. Tanta Medical Journal *51*, 34. https://doi.org/10.4103/tmj.tmj_23_22.

33. Bunaciu, A.A., Aboul-Enein, H., and Fleschin, Ş. (2015). Vibrational Spectroscopy in Clinical Analysis. Applied Spectroscopy Reviews *50*. https://doi.org/10.1080/05704928.2014.955582.

34. Alimagham, F.C., Hutter, D., Marco-García, N., Gould, E., Highland, V.H., Huefner, A., Giorgi-Coll, S., Killen, M.J., Zakrzewska, A.P., Elliott, S.R., et al. (2021). Cerebral Microdialysate Metabolite Monitoring using Mid-infrared Spectroscopy. Anal. Chem. *93*, 11929–11936. https://doi.org/10.1021/acs.analchem.1c01149.

35. Tian, W., Wang, D., Fan, H., Yang, L., and Ma, G. (2018). A Plasma Biochemical Analysis of Acute Lead Poisoning in a Rat Model by Chemometrics-Based Fourier Transform Infrared Spectroscopy: An Exploratory Study. Front. Chem. *6*. https://doi.org/10.3389/fchem.2018.00261.

36. Huber, M., Kepesidis, K.V., Voronina, L., Božić, M., Trubetskov, M., Harbeck, N., Krausz, F., and Žigman, M. (2021). Stability of person-specific blood-based infrared molecular fingerprints opens up prospects for health monitoring. Nat Commun *12*, 1511. https://doi.org/10.1038/s41467-021-21668-5.

37. Ge, R., and Zou, J. (2016). Rich Component Analysis. In Proceedings of The 33rd International Conference on Machine Learning (PMLR), pp. 1502–1510.

38. Lanthier, N., Rodriguez, J., Nachit, M., Hiel, S., Trefois, P., Neyrinck, A.M., Cani, P.D., Bindels, L.B., Thissen, J.-P., and Delzenne, N.M. (2021). Microbiota analysis and transient elastography reveal new extra-hepatic components of liver steatosis and fibrosis in obese patients. Sci Rep *11*, 659. https://doi.org/10.1038/s41598-020-79718-9.

39. Zhang, X., Gong, Y., and Sun, C. (2025). The interplay between trace element zinc and chronic liver diseases: Still water run deep. Journal of Functional Foods *127*, 106784. https://doi.org/10.1016/j.jff.2025.106784.

21/08/2025 12:26:00

FIGURE LEGENDS

Figure 1. The high-fat, high-carbohydrate diet induces a heterogeneous steatohepatitis. (A) mRNA level of Fsp27 (CT) depending on the experimental groups. **(B)** Hepatic triglyceride content (mg/g of liver) depending on the experimental groups. **(C)** Histological quantification of steatosis in hepatocytes (% of cells) depending on the experimental groups. *a* means that HFHC is statistically different from other groups, and *b* means that the IRON+HFHC group is statistically different from other groups. **(D)** Principal component analysis (PCA) of three steatosis-related variables: histological steatosis score, hepatic triglyceride concentration, and Fsp27 mRNA expression. **(E)** Pearson's r coefficients between PCA coordinates (from panel D) and five categories of biological variables. The figure shows the 95% confidence intervals of the correlations for: *(1)* blood markers of hepatic injury, *(2)* variables describing hepatic lipid accumulation, *(3)* fibrosis-associated variables, *(4)* inflammation-related markers, and *(5)* iron metabolism-related variables. The blue points correspond to variables that are statistically associated with PC1.

Figure 2. A multi-modal approach appears essential to encompass all the information in the dataset. (A) Mantel test results comparing the sample structure defined by steatosis-related variables with that of other datasets. A greater deviation from the null distribution indicates a higher degree of similarity between the sample structures. In other words, it means that datasets share information with steatosis-related variables. **(B)** Mantel test results assessing structural similarity between blood marker profiles and other datasets. In this case, it means that datasets share information with serum biochemical variables.

Figure 3. Comparative predictive performance (RMSE) of the four integration strategies for hepatic steatosis prediction. (A) Predictive performances from models based on a single type of data. **(B)** *Strategy 1: Early Integration*. Predictive performances from Extreme Gradient Boosting (XGBoost) and a random forest model are trained on all datasets combined into a single input. **(C)** *Strategy 2: Late Integration*. Predictive performances from Random Forest models trained independently on each dataset (blood markers, mid-infrared (MIR) spectroscopy, and serum metallome). A linear model is then trained to integrate the three predictions into one. **(D)** *Strategy 3: Mixed Integration*. This approach reduces complexity through independent transformations applied to each dataset. Specifically, Kernel PCA and Robust PCA were performed separately on each data modality, and the resulting latent space coordinates for each sample were then concatenated to form the explanatory variables of the Random Forest models. **(E)** *Strategy 4 (New): Sequential Integration.* Predictive performances from Sequential Random Forest models trained on residuals from the previous RF model to integrate complementary information from multiple datasets. The colour indicates the statistical significance of predictive performance based on the integration strategies compared to the predictive performance of the model trained only on serum markers (light green box). Statistically significant between integration strategies: *a*: $p<0.05$ compared to Early Integration, *b*: $p<0.05$ compared to Late Integration, *c*: $p<0.05$ compared to Mixed Integration. Multiple paired *t*-tests were performed, and the resulting *p*-values were corrected using the Bonferroni method.

TABLES

Clinical features	CTL	HFHC	IRON	IRON + HFHC
Body weight (g)	32.6 (+/- 3.8)	46.1 (+/- 7.0) *a*	31.1 (+/- 1.8) *b*	36.0 (+/- 4.9) *a,b,c*
Liver weight (g)	1.3 (+/- 0.24)	2.1 (+/- 0.7) *a*	1.8 (+/- 0.21) *a,b*	2.1 (+/- 0.47) *a,c*
Liver weight (% of BW)	4.14 (+/- 0.47)	4.66 (+/- 0.86)	5.72 (+/- 0.56) *a,b*	5.89 (+/- 0.61) *a,b*
Peri-epididymal weight (g)	0.74 (+/- 0.37)	2.75 (+/- 1.04) *a*	0.42 (+/- 1.8) *b*	1.08 (+/- 0.85) *b,c*
Peri-epididymal weight (% BW)	1.99 (+/- 1.03)	5.33 (+/- 2.45) *a*	1.25 (+/- 0.59) *b*	2.87 (+/- 1.85) *c*
Transferrin saturation (%)	39.5 (+ /- 9.7)	38.5 (+/- 8.7)	70.9 (+/- 16) *a,b*	51.5 (+/- 13) *a,b,c*
Serum Iron	19.6 (+/- 5.2)	21.9 (+/- 4.2)	32.6 (+/- 5.7) *a,b*	24.9 (+/- 5.4) *a,c*
Serum triglycerides (mmol/L)	0.86 (+/- 0.29)	1.31 (+/- 0.57) *a*	1.20 (+/- 0.24) *a*	1.68 (+/- 0.5) *a,b,c*
Total cholesterol (mmol/L)	2.5 (+/- 0.6)	3.8 (+/- 0.8) *a*	2.4 (+/- 0.2) *b*	3.7 (+/- 0.6) *a,c*
Glycemia (mmol/L)	17.4 (+/- 4)	21.4 (+/- 3 .9) *a*	17.9 (+/- 2.2) *b*	21.5 (+/- 5.1) *a,c*
ASAT (UI/L)	78.7 (+/- 30.4)	99.6 (+/- 49.1)	124 (+/- 68)	124 (+/- 53) *a*
ALAT (UI/L)	27.5 (+/- 15.8)	58 (+/- 43) *a*	54.9 (+/- 41.2) *a*	57 (+/- 40.6) *a*
PAL (UI/L)	50.9 (+/- 8.8)	44.2 (+/- 16.8)	58 (+/- 10.6) *b*	43.6 (+/- 13) *c*
CK (UI/L)	320 (+/- 209)	304 (+/- 246)	387 (+/- 328) *a,b*	465 (+/- 307) *a,b*

Table 1. Main morphological and serum biomarker data. Data shown are mean ± SD. ASAT: Aspartate aminotransferase; ALAT: Alanine aminotransferase; PAL: Phosphatase alkaline; CK: Creatin kinase. Statistically significant differences: *a* vs CTL, *b* vs HFHC, and *c* vs IRON. Multiple Wilcoxon tests with Bonferroni correction.

VARIABLES		INTERPRETATION	REFERENCES
BLOOD MARKERS			
CHOLESTEROL	↑	Serum free cholesterol is associated with steatosis severity.	Elsawy et al., 2023[32]
MIR			
1230 CM-1	↑	Vibration P=O, C–O Nucleotides, phospholipids, organic phosphates.	Bunaciu et al., 2015[33]
1180 CM-1	↑	Vibration C–O, C–C Glucose, lactate, pyruvate, simple sugars.	Alimagham et al., 2021[34]
950 CM-1	↑	Sugar ring vibration, C–C Cyclic carbohydrates, ribose, phosphorylations.	Tian et al., 2018[35]
840 CM-1	↑	C–H out-of-plane, rings Nucleic acids, polysaccharides, cyclic proteins	Hubert et al., 2021[36]
METALLOME			
ZINC	↑	Zinc metabolism is associated with NAFLD. Overload can lead to toxicity.	Zhang et al., 2025[39]
COPPER	↑	Copper overload is associated with steatosis.	Aigner et al., 2015[17]

Table 2. Key variables contributing to the prediction of the synthetic outcome summarizing steatohepatitis in mice. The second column is the sense of the variation of the variable depending on the severity of the steatosis.